5708 *Biochemistry* **2009,** *48,* 5708–5720
DOI: 10.1021/bi900511b

BIOCHEMISTRY
including biophysical chemistry & molecular biology
Article

Magnetic Interactions Sense Changes in Distance between Heme b_L and the Iron−Sulfur Cluster in Cytochrome bc_1[†]

Marcin Sarewicz,* Małgorzata Dutka, Wojciech Froncisz, and Artur Osyczka*

Department of Biophysics, Faculty of Biochemistry, Biophysics and Biotechnology, Jagiellonian University, Kraków, Poland

Received March 25, 2009; Revised Manuscript Received May 4, 2009

ABSTRACT: During the operation of cytochrome bc_1, a key enzyme of biological energy conversion, the iron−sulfur head domain of one of the subunits of the catalytic core undergoes a large-scale movement from the catalytic quinone oxidation Q_o site to cytochrome c_1. This changes a distance between the two iron−two sulfur (FeS) cluster and other cofactors of the redox chains. Although the role and the mechanism of this movement have been intensely studied, they both remain poorly understood, partly because the movement itself is not easily traceable experimentally. Here, we take advantage of magnetic interactions between the reduced FeS cluster and oxidized heme b_L to use dipolar enhancement of phase relaxation of the FeS cluster as a spectroscopic parameter which with a unique clarity and specificity senses changes in the distance between those two cofactors. The dipolar relaxation curves measured by EPR at Q-band in a glass state of frozen solution (i.e., under the conditions trapping a dynamic distribution of FeS positions that existed in a liquid phase) of isolated cytochrome bc_1 were compared with the curves calculated for the FeS cluster occupying distinct positions in various crystals of cytochrome bc_1. This comparison revealed the existence of a broad distribution of the FeS positions in noninhibited cytochrome bc_1 and demonstrated that the average equilibrium position is modifiable by inhibitors or mutations. To explain the results, we assume that changes in the equilibrium distribution of the FeS positions are the result of modifications of the orienting potential gradient in which the diffusion of the FeS head domain takes place. The measured changes in the phase relaxation enhancement provide the first direct experimental description of changes in the strength of dipolar coupling between the FeS cluster and heme b_L.

Cytochrome bc_1 is an integral part of several respiratory and photosynthetic electron transport systems. The catalytic core of this multicomponent transmembrane protein embeds two chains of cofactors (the high-potential "c-chain" comprising the iron−sulfur center FeS,[1] heme c_1, and cytochromes c and the low-potential "b-chain" comprising heme b_H, heme b_L, and quinone of the Q_i site) that meet at the charge-separating catalytic Q_o site (*1*). The structural arrangement of cofactors around the Q_o site is highly conserved throughout all members of cytochrome *bc* family as shown by resolutions of crystals of mitochondrial and bacterial cytochromes bc_1 (*2*−*7*) and plant cytochromes b_6f (*8*, *9*). Undoubtedly, the conservation in design is in part imposed by the conservation in function; all of these systems were developed to reversibly convert the redox free energy of quinone/plastoquinone and cytochrome *c*/plastocyanin substrates into a transmembrane electric potential and pH gradient. This is accomplished through a joint action of the two chains which use the Q cycle mechanism (*10*) to connect functionally the two quinone binding sites (Q_o and Q_i).

An integral part of the Q cycle involves a reversible two-electron oxidation of quinol in the catalytic Q_o site with one electron delivered into the c-chain and the other into the b-chain. This reaction, unique in biology, relies on the joint action of the FeS center and heme b_L, which are the first and immediate cofactors from either of the chains to participate in the electron transfer from/to quinol/quinone. Just how this reaction is catalyzed is not clear and is intensely debated (see examples in refs (*11*−*16*)). One of the remaining controversies surrounds the role of the large-scale motion of the FeS head domain (*17*), which during the catalytic cycle moves between the states where the FeS cluster approaches the Q_o site (Q_o position) and the states where it approaches heme c_1 (c_1 position) (Figure 1). Because of the change in distance between cofactors, these positions are mutually exclusive in terms of the electron transfer they support: in the Q_o position, the FeS cluster exchanges electron just with the bound quinone substrate, while in the c_1 position, it exchanges electron just with heme c_1.

[†]This work was supported by The Wellcome Trust International Senior Research Fellowship to A.O.

*Corresponding authors. Phone: +48-12-664-6348. Fax: +48-12-664-6902. E-mail: artur.osyczka@uj.edu.pl; marcin.sarewicz@gmail.com.

[1]Abbreviations: FeS, [2Fe-2S] iron−sulfur; CW EPR, continuous wave electron paramagnetic resonance; EDTA, ethylenediaminetetraacetic acid; ESE, electron spin echo; ED EPR, echo-detected electron paramagnetic resonance spectra; ESEEM, electron spin echo envelope modulation; IR, inversion recovery; T_1, spin−lattice relaxation time; T_M, phase memory time; Δ, dipolar splitting; $P_{1/2}$, microwave power for which signal amplitude is half of the signal in the absence of saturation; *R. capsulatus, Rhodobacter capsulatus.*

 Published on Web 05/05/2009

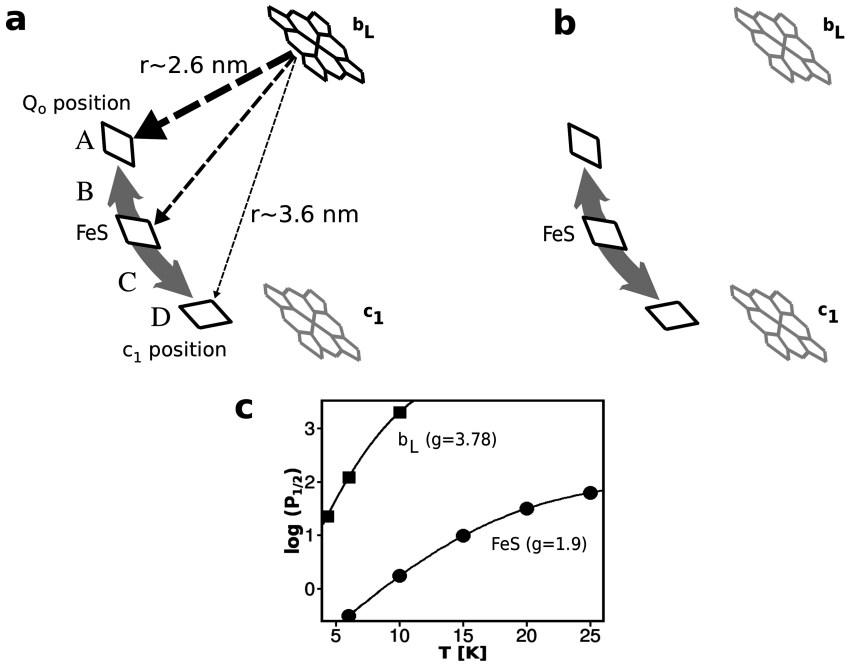

FIGURE 1: Changes in distances between the FeS cluster and hemes c_1 and b_L in cytochrome bc_1. The movement of the FeS head domain changes the length of interspin vector **r** between the center of the FeS cluster plane (black rhombus) and the Fe metal of heme b_L from ~2.6 nm (Q_o position) to ~3.6 nm (c_1 position). (a) Addition of ascorbate produces paramagnetic form of the FeS cluster and heme b_L (black) and diamagnetic form of heme c_1 (gray). (b) Sodium dithionite reduces all cofactors leaving the paramagnetic FeS cluster (black) and diamagnetic hemes (gray). Magnetic interactions (dashed arrows) are only possible between the paramagnetic centers (heme b_L and the FeS cluster) so they are present exclusively in (a) but not in (b). These long-range interactions depend on **r** (the widths of the arrows are proportional to the strength of the interaction) and can be detected by relaxation measurements when one of the centers is a fast-relaxing and the other is a slow-relaxing species. A, B, C, and D refer to four crystal positions of FeS head domain used in simulations of dipolar curves (see Experimental Procedures and Supporting Information). (c) compares the relaxation behavior of heme b_L (squares) and the FeS cluster (circles) expressed as $P_{1/2}$ (mW) determined from power saturation CW EPR experiments at X-band at $g = 3.78$ (g_z transition of heme b_L) and $g = 1.9$ (g_y transition of the FeS cluster).

Although the motion of the FeS head domain was first implicated from various crystal structures of cytochromes bc_1, the possibility of the existence of some sort of a catalytic switch (reminiscent of motion) has been suggested before the crystal structures were known (*18*). Crystallography revealed that the FeS head domain of the FeS subunit shows different positions in different crystals with respect to the other subunits of the catalytic core (cytochrome *b* and c_1 subunits) depending on whether and what type of the Q_o site inhibitor is used. When inhibitors such as stigmatellin are used, the FeS head domain is seen in the state within the Q_o site, which is related to the fact that this inhibitor forms hydrogen bonds with one of the histidines coordinating the FeS cluster (*4*, *5*). This arrests the head domain at the Q_o site and forbids the movement. Other inhibitors, such as myxothiazol, do not form the hydrogen bonds with the FeS head domain and allow its movement. When myxothiazol is used, the FeS head domain is seen in positions different from that seen in crystals with stigmatellin, close or more remote from the Q_o site (*3*, *19*). Still other positions are seen when cytochrome bc_1 is crystallized in the absence of any inhibitors (*3*, *4*).

Although the necessity of the movement in the cytochrome bc_1 catalysis has been well established through a number of biochemical, biophysical, and kinetic studies (*17*, *20*−*22*), the meaning of the various positions revealed by crystals remains unclear. This is partly because the movement itself is not easily traceable experimentally and has never been observed directly. The so far existing techniques rely mainly on analysis of CW EPR spectra of ordered systems (*23*−*27*). Those techniques, despite experimental challenges related to both the preparation of the samples and the interpretation of the data, provided a lot of valuable information on the angular dependence of the amplitude of g_x transition of the FeS cluster under many conditions (*23*−*27*).

To get an insight that does not rely on the changes in the shape of CW EPR spectra, we have considered a possibility of applying a method that exploits an intrinsic physical process sensitive to the change in distance between the cofactors. With such a method, the measurements of nonordered systems (i.e., in powders) would provide us with a spectroscopic parameter directly correlated with the motion-related changes in the FeS head domain positions.

Because the metal cofactors of cytochrome bc_1 possess magnetic properties in certain redox states, it seemed reasonable to explore the method that measures dipole−dipole interactions between the metal centers. Typically, those interactions are examined using EPR spectroscopy with which distances between paramagnetic centers up to about 7 nm can be determined (*28*−*38*). Examples of the pairs of the redox centers for which distances were measured include the heme *b*−3Fe4S cluster of complex II (*28*), tyrosine radical−nonheme Fe(II) of PSII (*31*), tyrosine radical−Mn cluster of PSII (*39*), Cu_A−heme *a* of cytochrome oxidase (*30*), Cu^{2+}−heme of cytochrome *f* in cytochrome b_6f (*37*), and cytochrome *c*/cytochrome oxidase (in this case estimation of distance distribution in the interprotein complex was reported (*38*)). In the case of cytochrome bc_1, early EPR examination of mitochondrial enzyme allowed to approximate a spatial organization of its redox active centers revealing existence of weak spin−spin interactions between the FeS center, heme b_{566} (b_L), and heme c_1 (*40*).

In this work we applied pulse EPR to examine the interaction between the FeS cluster and heme b_L of cytochrome bc_1 that takes place within the range of approximately 2.6−3.6 nm (Figure 1a).

We first identified the relaxation process in which the magnetic interactions between those centers are manifested. Then, by measuring the distance-dependent impact of the heme relaxation on the relaxation of the FeS cluster, we were able to describe the equilibrium distribution of the FeS positions in noninhibited cytochrome bc_1 and compare it with the distribution present in the inhibitor-induced states and in the mutant form sterically arresting the FeS head domain at the Q_o site. We explained the results using a diffusion-based mode of the FeS head domain motion and linked the changes in the equilibrium distribution of the FeS positions with modifications of the orienting potential gradient in which the diffusion takes place.

EXPERIMENTAL PROCEDURES

Biochemical Procedures. Cytochrome bc_1 was isolated from appropriate strains of purple bacterium *Rhodobacter capsulatus* (*20*, *41*) according to the procedure described in ref (*42*). Concentration of cytochrome bc_1 was determined from ascorbate-reduced minus ferricyanide-oxidized difference optical spectra using cytochrome c_1 extinction coefficient $\varepsilon_{551-542nm} = 20$ mM^{-1} cm^{-1} (*42*). Heme c_1 and the FeS cluster were reduced with 1 mM sodium ascorbate. To reduce all metal centers in cytochrome bc_1, a small amount of solid sodium dithionite was added to the sample. Samples with inhibitors antimycin, myxothiazol, or stigmatellin were prepared by addition of a 6-fold molar excess of the corresponding inhibitor over cytochrome bc_1 monomers. For continuous wave EPR (CW EPR) measurement at X-band approximately 160 μL of 50 μM cytochrome bc_1 solution was transferred to 4 mm (OD) quartz tubes and frozen by immersion in liquid nitrogen. In the case of Q-band measurements 10 μL of 280 μM cytochrome bc_1 was transferred into a 1.6 mm (OD) quartz tube and quickly immersed in liquid nitrogen.

EPR Measurements. All experiments were performed in 50 mM bicine buffer, pH 8.0, 100 mM NaCl, 1 mM EDTA, and 20% glycerol. The use of bicine minimizes changes of buffer pH due to freezing the sample (*43*), and the presence of cryoprotectant (glycerol) is obligatory to prevent the aggregation of proteins and ice formation in the water solutions upon freezing (*44*). The measurements were carried out on a Bruker Elexsys-E580 X/Q-band spectrometer. CW EPR spectra at X-band (~9.4 GHz) were measured at 20 K using a Bruker SHQ4122 resonator equipped with an ESR900 cryostat (Oxford Instruments). Temperature was regulated with an ITC503S controller (Oxford Instruments). Settings were as follows: microwave power 2 mW, modulation amplitude/frequency 15 G/100 kHz, time constant 20.48 ms, sweep width/time 1600 G/42 s, and frequency 9.38 GHz.

Pulse experiments were performed at Q-band using a Bruker SuperQFT-u module that shifts the operating frequency from 9.5 to ca. 33.6 GHz. The spectrometer was equipped with an overcoupled Bruker ER5107D2/0501 Q-band resonator inserted in a CF935 helium cryostat (Oxford Instruments). Echo-detected EPR spectra (ED EPR) were recorded by integration of the electron spin echo signal (ESE) generated by two-pulse sequence $(\pi/2-\tau-\pi) \pm 62$ ns around the maximum with two-step phase cycling at different magnetic field induction B_0. Pulse lengths were set to 20 and 40 ns for $\pi/2$ and π pulse, respectively.

Each measurement was repeated at least four times, using samples that were obtained from separate isolations of cytochrome bc_1. All of the Q-band measurements were highly reproducible, and no variation between different preparations was observed.

Analysis of Phase Relaxation Rates. Phase relaxation rates were determined from the electron spin echo decay curve recorded by integration of the echo signal for increasing separation (τ) between pulses. The interpulse time τ increased in 4 ns steps, and the curves were digitalized with 1024 points. Empirical parameter, phase memory time T_M that describes all processes that lead to the loss of coherence of spin precession, was determined from fitting the stretched exponent function (*33*, *35*):

$$A(t) = a \exp\left[-\left(\frac{t}{T_M}\right)^{\beta}\right] + y0 \qquad (1)$$

to the recorded ESE decays using the Levenberg−Marquardt algorithm.

The measured signals decay very quickly, especially in ascorbate-reduced samples. Due to unavoidable long spectrometer dead time we can record only the part of the overall decay process. The pronounced echo envelope modulation caused by coupling of the cluster electron spin to the neighboring nuclear spins (*45*) makes the fit very sensitive to the onset point of the fitting. This raises the concern as to where to set the zero point of time axis in the fitting procedure. We observed that setting the zero point in time to the start of the relaxation process makes the fitting eq 1 to ESE decay curves unstable and the obtained parameters become sensitive to both the onset of the fit and the length of the tail of the measured curves, especially for ascorbate-reduced samples. This is because the estimated T_M, after correction for the dead time, may become shorter than the dead time. Thus, to improve the stability of the fitting procedure, we decided to set the zero point in time to the start of the acquisition process. For all samples, the reliable fits were judged by the presence of the symmetrical ESEEM signal on residuals. Also, the initial several nanoseconds of the decay, where the modulations were deepest, were omitted, and only the remaining portion of the curves was fitted. With this setting, the estimated T_M should be considered as an *empirical parameter* used for comparison of the rate of the decay due to interaction with paramagnetic heme b_L in different samples, rather than a description of a true phase memory time. Note that for simulation of the dipolar decays the zero point in time was obligatorily set to the beginning of the phase relaxation process (see below).

Recorded ESE decay curves are the product of intrinsic phase relaxation (V_i), ESE envelope modulations (V_{ESEEM}), and dipolar relaxation (V_{dip}) (*38*, *46*). To extract V_{dip} from experimental ESE decays, division of the curves measured in the presence and absence of interaction with fast relaxing metal was applied. Prior to division, the offset ($y0$ value in eq 1) was subtracted from the measured ESE decay curves. Then the curves of ascorbate-reduced samples were divided by the curves of dithionite-reduced samples obtained for the same temperatue. The resulting pure dipolar curves were normalized and fitted with a single exponent to estimate the ratio of the offset (a deviation of the ending part of the curve from zero) to amplitude.

The changes of phase relaxation rate ($1/T_M$) of the FeS cluster between 12 and 26 K were approximated by fitting the third order of polynomial to the dithionite-reduced sample or the sum of third order polynomial and Lorentzian function to the ascorbate-reduced samples. The fits obtained for dithionite-reduced cytochrome bc_1 were subtracted from those obtained for ascorbate-reduced samples, and the resulting curves were numerically integrated from 12 to 26 K. This yielded values of integrated

area between the curves that, for reasons given below, were used in comparison of the extent of enhancement in various samples.

The dipolar enhancement of phase relaxation is effective within 12−26 K. Within this range the coincidence between the spin−lattice relaxation of heme b_L ($1/T_1^{heme}$) and dipolar coupling between the FeS cluster and heme b_L takes place. Assuming that temperature dependence of $1/T_1^{heme}$ is the same for all samples, it influences the width of the temperature dependence of $1/T_M$ in the same way. Thus the observed in our samples different effectiveness of dipolar enhancement comes from differences in dipolar coupling, which depends on a specific distance and orientational distribution of interacting spin pairs. Simulations of dipolar decays show that the smaller value of the area is expected for the samples with greater average distance between magnetically coupled spins of the FeS cluster and heme b_L.

Analysis of Spin−Lattice Relaxation Rates. Spin−lattice relaxation rates were determined with the use of inversion recovery (IR) three-pulse sequence ($\pi-\tau-\pi/2-300$ ns$-\pi$) with the increasing τ. Duration of $\pi/2$ and π pulses were set to 20 and 40 ns. Microwave power was set to 19.5 mW, and the four-step phase cycling was applied to remove unwanted echoes from measured signal. All measured IR curves where fitted with either single exponent, sum of two exponents, or single stretched exponent function with the zero point in time set to the beginning of the relaxation. For all measured samples the IR curves could not be well fitted with a single exponent. Reasonably good fits were obtained with the use of either sum of two exponents or single stretched exponent. The nonexponential shape of IR curves is usually attributed to a contribution from spectral diffusion that often obscures intrinsic longitudinal relaxation rates determined from inversion recovery (*35*, *44*). In order to examine this contribution, the spin−lattice relaxation rates for dithionite-reduced samples in the presence of stigmatellin at 15 and 19.5 K were measured by three different methods. The first method was standard IR which uses a single inverting π pulse. In the second method, the first π pulse was replaced with either $14\,\pi$ or $14\,\pi/2$ pulses (picket fence) (*28*). The third method was echo-detected saturation recovery in which the first inverting π pulse was replaced with a single long (21 μs) saturating pulse. We found no differences in fitted parameters to the curves registered by these three methods. Therefore, we concluded that spectral diffusion is not responsible for nonexponential IR curves. This nonexponential character suggests the presence of a distribution of relaxation rates of the FeS cluster. Therefore, we fitted all curves with stretched exponent function that allowed us to describe the shape of the curve with the minimum number of free parameters (τ_{ww} and β) (*47*).

The stretching parameter that was obtained from fitting IR curves fulfilled the condition $0 < \beta \leq 1$ in all cases; therefore, the curves can be assumed to represent Williams−Watts function that usually encompasses the large different possible distributions of exponents. In order to calculate the average spin−lattice relaxation time constant $\langle\tau\rangle_{ww}$, the following formula was applied (*48*):

$$T_1 = \langle\tau\rangle_{ww} = \Gamma\left(\frac{1}{\beta}\right)\frac{\tau_{ww}}{\beta} \qquad (2)$$

where Γ is gamma function.

Temperature dependences of spin−lattice relaxation rates $1/T_1$ between 5 and 40 K were fitted assuming the contribution from direct, Orbach, and Raman processes (*35*):

$$\frac{1}{T_1} = A_{dir}T + A_{orb}\frac{E_{orb}^3}{\exp(E_{orb}T^{-1})-1} + A_{ram}\left(\frac{T}{\theta_D}\right)^9 J_8\left(\frac{\theta_D}{T}\right)$$

where A_{dir}, A_{orb}, and A_{ram} are coefficients for direct, Orbach, and Raman process, respectively, E_{orb} is the energy difference between the ground and low-lying excited state, θ_D is Debye temperature, and J_8 is the transport integral. Spin−lattice relaxation rate of the FeS cluster in the temperature range 12−26 K was well described assuming the dominant Orbach process.

Simulation of Dipolar Decay Curves. Simulation of the dipolar curves of ESE decay were performed using a home-written Matlab program (The MathWorks). The program was based on the theory of spectral diffusion in spin-coupled systems originally developed by Zhidomirov and Salikov (*34*, *38*, *49*). For the calculations of the dipolar ESE decay curves, knowledge of the principal *g*-tensor values and spin−lattice relaxation rate of the fast-relaxing spin (heme b_L in our case) is required. Unfortunately, only g_z transition (related to the molecular axis perpendicular to the heme plane) can be measured by X-band CW EPR spectra, and since the remaining g_y and g_x values have not been precisely determined (*40*, *50*), we assumed that heme b_L possesses the axial symmetry defined by two *g*-tensor values: $g_\perp = 3.78$ and $g_{||} = 1.6$. Additionally, we were unable to measure relaxation rate of this heme at Q-band due to the extremely weak signal that gives no detectable ESE, even at temperatures around 5 K. Those two missing parameters significantly limit the possibility to obtain quantitative information on the exact distribution of the positions of the FeS cluster in respect to the heme b_L from simulations of the dipolar curves. Nevertheless, we were able to compare the calculated dipolar curves with experimental data assuming the relaxation rate of heme b_L between 100 and 0.1 MHz.

Contribution to the dipolar echo decay comes from the resonant spins of the FeS cluster, selected by the exciting microwave pulse within ±4.5 G around the resonant magnetic field B_0 (i.e., all spins with g_{eff} fulfilling the resonance conditions within this selected range). Consequently, all of the selected orientations of interspin vector **r** connecting the center of the FeS cluster and iron of heme b_L, with respect to the direction of external magnetic field $\mathbf{B}_0$ vector, were taken for calculations. Spatial orientations and distances between the FeS cluster and heme b_L were extracted from four PDB structures of mitochondrial cytochrome bc_1 referred as A (r = 2.64 nm) (entry 1ezv.pdb), B (r = 3.12 nm) (entry 1bgy.pdb), C (r = 3.41 nm) (structure with myxothiazol from ref (*3*)), and D (r = 3.55 nm) (entry 1be3.pdb) positions (see Figures 1a and S1 Supporting Information). All calculations were carried out in the reference frame defined by the principal **g** tensor axes (GRF) of the FeS cluster. The coordinates of the **r** vector, retrieved from the PDB data, are given in a laboratory reference frame (LAB). Thus the consecutive unitary transformations of **r** from LAB to the molecular reference frame (MOL) and then from MOL to GRF were applied. Different rotational matrixes were calculated for A, B, C, and D positions. The final transformation from MOL to GRF used the rotational matrix determined by Bowman et al., who observed two magnetically distinguished monomers of the FeS cluster in cytochrome bc_1 (*51*). Calculation of g_{eff} for the powder-like distribution of the FeS orientation was

performed using functions implemented in the EASYSPIN package (*52*).

RESULTS

Fast- and Slow-Relaxing Metal Centers of the Q_o Site. During the catalytic cycle of cytochrome bc_1 the iron−sulfur head domain moves between the Q_o site and cytochrome c_1 (Q_o and c_1 positions in Figure 1a) to perform its electron relay function. This movement is inherently associated with changes in distance between the FeS center and other redox centers of cytochrome bc_1. As revealed by different crystal structures of cytochrome bc_1 (*2*−*5*), the distance between the FeS cluster and the iron of heme b_L can be distributed over 1 nm, changing from approximately 2.6 nm when the FeS head domain is in the Q_o position to approximately 3.6 nm when the FeS head domain is in the c_1 position (Figure 1a). In principle, such a change should modulate magnetic interactions between the metal centers provided they are paramagnetic.

The low-spin iron in hemes b_L and c_1 display paramagnetism ($S = {}^1/_2$) only when the heme is in the oxidized state. On the other hand, the antiferromagnetically coupled high-spin Fe of the FeS cluster forms a paramagnetic molecule when the cluster is in the reduced form (*53*). The equilibrium redox midpoint potential of heme b_L is over 400 mV lower than those of heme c_1 and the FeS cluster (at pH 7 it is −120 mV vs +320 mV). Because of such large difference in potentials it is easy to set conditions with which both the FeS cluster and heme b_L are paramagnetic (being reduced and oxidized, respectively) while heme c_1 remains diamagnetic (reduced) (Figure 1a); they are obtainable by just addition of ascorbate which reduces the FeS cluster and heme c_1 but not heme b_L. We expect that under those conditions the FeS cluster might sense an electron magnetic moment originating from the metal of heme b_L (but not from heme c_1 which remains EPR silent). In contrast, reducing all metal-containing cofactors by dithionite eliminates magnetic moments of both hemes abolishing any interactions with the paramagnetic FeS cluster (Figure 1b).

One of the most sensitive spectroscopic effects that sense the interaction of the two magnetic moments is an impact of a fast-relaxing metal on the relaxation of more slowly relaxing species. Figure 1c shows a temperature dependence of the $P_{1/2}$ parameter (proportional to $\gamma^{-2}(T_1T_2)^{-1}$) determined from the power saturation of the X-band CW EPR signal of the FeS cluster (g = 1.90) and heme b_L (g = 3.78). It is evident that at temperatures above 10 K $P_{1/2}$ of heme b_L is over 3 orders of magnitude larger than that of the FeS cluster. Thus, heme b_L and the FeS cluster can be considered as fast- and slow-relaxing paramagnets, respectively. For that reason, the relaxation of iron of heme b_L is expected to enhance the relaxation of the FeS cluster in a manner that strongly depends on the distance between the two metal centers.

Echo-Detected EPR Spectra of Oxidized and Reduced FeS Cluster. Figure 2 sets the Q-band ED EPR spectra of the FeS cluster in the context of the commonly known X-band CW EPR. At X-band, CW EPR spectra of reduced FeS cluster show three principal transitions, g_z, g_y, and g_x, of the rhombic symmetry of the cluster (Figure 2). In isolated native cytochrome bc_1 of *R. capsulatus* those transitions are 2.03, 1.90, and 1.78−1.76, respectively. The g_x transition has been found to be highly sensitive to many factors, including those related with the occupancy state of the Q_o site (*54*, *55*). We note that, as in our case, the g_x of around 1.77 has typically been observed in the isolated cytochrome bc_1 preparations without external quinone added (*56*). At Q-band, the spectra of the FeS cluster are approximately 3.5 times wider, as seen in ED EPR shown in Figure 2. The shape of those absorption-like spectra depends on separation time between $\pi/2$ and π pulses (τ) (Figure 2 compares spectra registered for τ of 200, 600, and 1000 ns). This is caused mainly by angular dependence of ESEEM. In addition, anisotropy of spin−spin and/or spin−lattice relaxation may contribute.

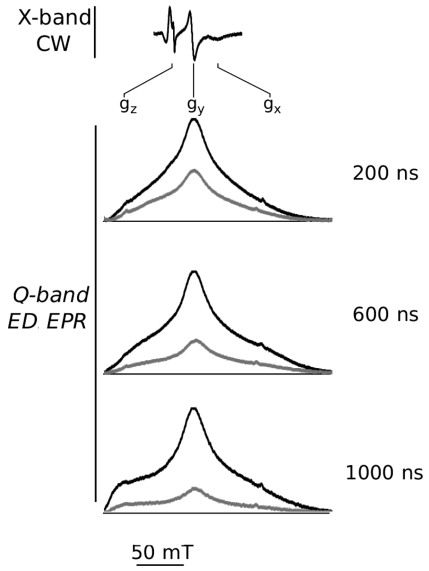

FIGURE 2: Q-band EPR spectra of the reduced FeS cluster in the isolated native cytochrome bc_1. Absorption-like ED EPR spectra were recorded by measuring the magnetic field dependence of echo amplitude exited by a pulse sequence $\pi/2-\tau-\pi$. Spectra obtained for three values of τ, 200, 600, or 1000 ns, are shown for dithionite- (black) and ascorbate-reduced (gray) samples. X-band CW EPR spectrum of FeS cluster is added to the top of the figure to compare the extent of Zeeman splitting of the rhombic spectrum at 9.35 (X-band) and 33.6 GHz (Q-band). g_z, g_y, and g_x denote the transitions related to the principal values of the g-tensor. CW EPR X-band spectrum is shifted to align g_y field position to the field value of g_y transition at Q-band.

Regardless of the τ used, large differences in both the shape and the amplitude of ED EPR are seen between the samples reduced with ascorbate and dithionite. For τ of 200 ns, the amplitude of ESE of the FeS cluster in ascorbate-reduced cytochrome bc_1 is approximately two times lower than that of dithionite-reduced cytochrome bc_1. This difference increases with τ; when τ exceeds 1000 ns, the signal of the ascorbate-reduced sample becomes barely measurable while this of the dithionite-reduced sample remains reasonably strong. In light of the discussion of Figure 1 (see paragraph above) we interpret the observed decrease in the ESE amplitude in the ascorbate- vs dithionite-reduced samples as a result of an enhancement of the cluster relaxation induced by magnetic interaction with oxidized heme b_L present in the ascorbate-reduced samples. We note that under those conditions the other heme b of the cytochrome b subunit (heme b_H) is also oxidized and paramagnetic and, thus, might contribute to the enhancement. However, since the distance between this heme and the FeS cluster is at least 1 nm larger than that of heme b_L and FeS cluster, and the relaxation of heme b_H is slower than that of heme b_L (data not shown), we expect that the contribution of heme b_L dominates the enhancement.

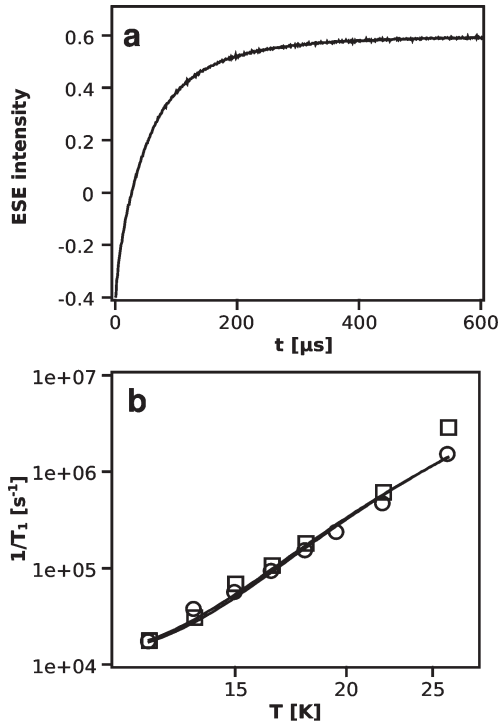

FIGURE 3: Effect of temperature and reduction state of heme b_L on spin−lattice relaxation rate of the FeS cluster in stigmatellin-treated cytochrome bc_1. (a) shows a typical Q-band inversion−recovery curve, registered at 12 K. (b) shows the temperature dependence of spin−lattice relaxation rate in ascorbate- and ditionite-reduced cytochrome bc_1 (squares and circles, respectively). Fits in (b) (solid lines) assume dominant Orbach process. Estimated Orbach energies of the FeS cluster for ascorbate- and dithionite-reduced samples are 128 and 133 K, respectively.

In principle, the enhancement of the FeS cluster relaxation may result from the shortening of spin−lattice relaxation of the cluster, phase relaxation of the cluster, or both. In order to determine which relaxation process is mostly affected, we performed the pulse measurements of spin−lattice relaxation time (T_1) and of phase relaxation time constant (T_M) of the cluster.

Spin−Lattice Relaxation of the FeS Cluster in Ascorbate- and Dithionite-Reduced Cytochrome bc_1. The spin−lattice relaxation time (T_1) of the FeS cluster was determined from the inversion recovery (IR) measurements at temperature range 12−31 K. Fitting the stretched exponent to the IR curve recorded at a given temperature (see Experimental Procedures), such as that shown in Figure 3a, yielded the τ_{ww}. The spin−lattice relaxation rates $1/T_1$ calculated from eq 2 were taken to construct the plots of temperature dependence of the relaxation rates. Figure 3b shows the plots obtained with ascorbate- and dithionite-reduced cytochrome bc_1 in the presence of stigmatellin. This inhibitor locks the FeS head domain at the Q_o position setting the conditions where the distance between the FeS cluster and heme b_L is the shortest; thus the strongest influence of this heme can be expected. Yet, the plots revealed no difference between the samples with reduced and oxidized hemes *b*, indicating that oxidized heme b_L does not influence the spin−lattice relaxation rate of the FeS cluster within the tested temperature range.

Electron Spin Echo Decay of the FeS Cluster in Ascorbate- and Dithionite-Reduced Cytochrome bc_1. The phase relaxation time constant (T_M) was examined by measuring the ESE decay, using a two-pulse Hahn sequence. Figure 4 shows typical ESE decay curves of the FeS cluster in isolated cytochrome bc_1 registered at g_z, g_y, and g_x transitions.

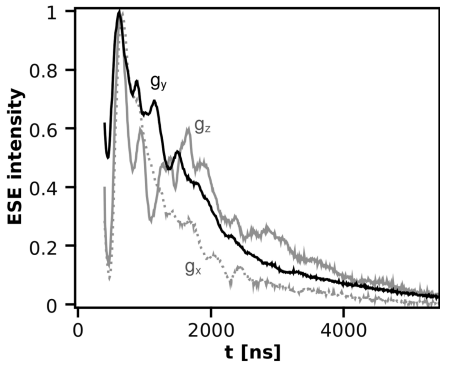

FIGURE 4: Anisotropy of the ESE decay curves of the FeS cluster. Electron spin echo decays were measured at Q-band at 15 K in native, noninhibited cytochrome bc_1 reduced with dithionite. The curves were registered at spectral positions corresponding to g_z (gray solid), g_y (black solid), and g_x (gray dotted) transitions.

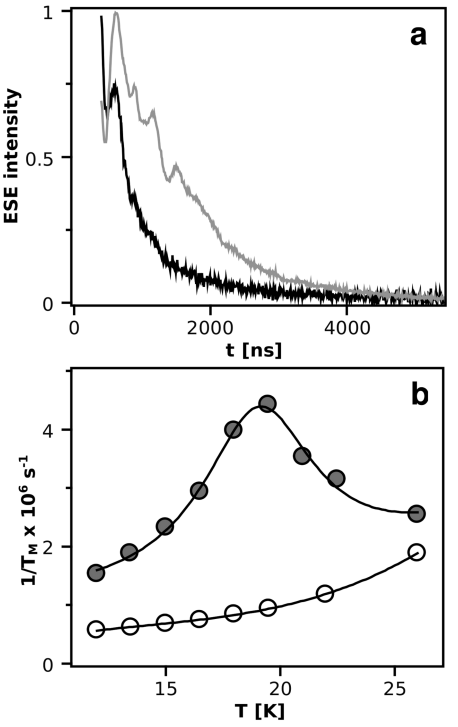

FIGURE 5: Influence of relaxation of heme b_L on phase relaxation rate of FeS cluster in the stigmatellin-treated native cytochrome bc_1. (a) Electron spin echo decay registered at Q-band at 19.5 K in dithionite-reduced (gray) and ascorbate-reduced (black) cytochrome bc_1. (b) Temperature dependence of phase relaxation rate defined as $1/T_M$ in dithionite-reduced (open circles) and ascorbate-reduced (closed circles) cytochrome bc_1. Solid lines represent a trend that was approximated by fitting the third order of polynomial to the dithionite-reduced sample or the sum of third order polynomial and Lorentzian function to the ascorbate-reduced samples.

Anisotropy of ESEEM signal in the ESE decay curves shown in Figure 4 leads to different modulation patterns obtained at different spectral positions. Since ESEEM obscures determination of the phase memory time, the least modulated curves at g_y were taken for further analysis. Those curves have the largest ESE amplitude, which additionally made them most suitable for T_M calculations.

Figure 5a compares ESE decay curves at g_y of the FeS cluster in ascorbate- and dithionite-reduced cytochrome bc_1 registered at 19 K. As in the spin−lattice relaxation measurements, the sample was treated with stigmatellin to ensure the shortest distance

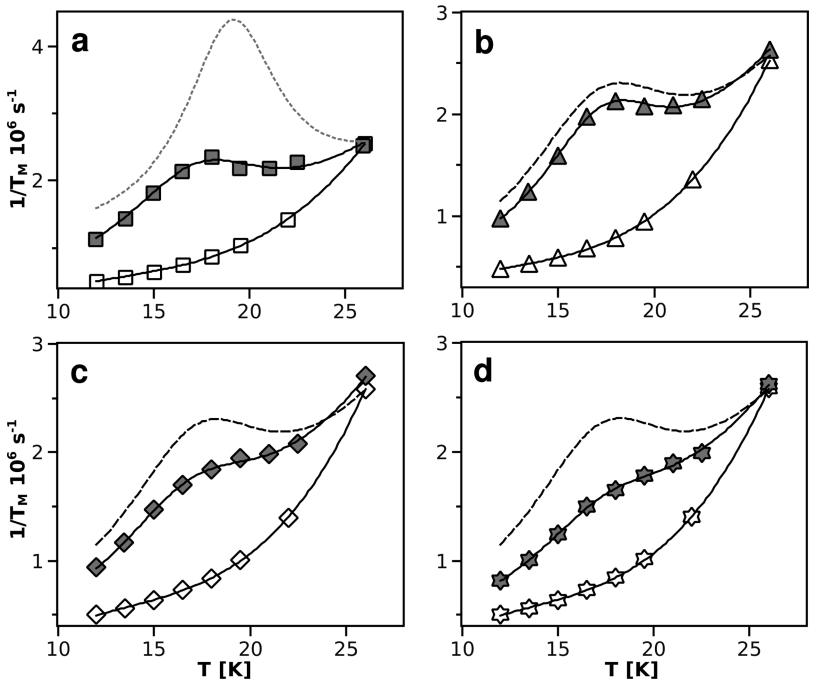

FIGURE 6: Comparison of the effect of inhibitors on the temperature dependence of phase relaxation rate of the FeS cluster in native cytochrome bc_1. Shown are data for ascorbate-reduced (closed symbols) and dithionite-reduced (open symbols) samples of noninhibited cytochrome bc_1 (a) and enzyme inhibited with myxothiazol (b), antimycin (c), or antimycin plus myxothiazol (d). For comparison, in (a) the dashed gray line shows data for ascorbate-reduced, stigmatellin-treated cytochrome bc_1 reproduced from Figure 5b; in (b−d) dashed lines show data for ascorbate-reduced noninhibited cytochrome bc_1 reproduced from (a).

between the FeS cluster and heme b_L. It is clear that ESE decays significantly faster in the ascorbate-reduced sample and consequently T_M obtained from fitting the experimental curve with the stretched exponent (see Experimental Procedures) is shorter. A detailed examination of the temperature dependence of ESE decay rate ($1/T_M$) in those samples is shown in Figure 5b. In the case of the dithionite-reduced sample, $1/T_M$ shows a weak and monotonic dependence on temperature in the range 12−26 K. On the other hand, in the ascorbate-reduced sample, $1/T_M$ increases with temperature reaching maximum at 19 K and then decreases. We interpret the difference between the two profiles shown in Figure 5b as indication that oxidized heme b_L present in the ascorbate-reduced sample enhances phase relaxation of the FeS cluster. This appears to be a resonance-type enhancement with a maximum point corresponding to temperature where the relaxation rate of heme b_L is equal to the strength of the dipolar coupling with the FeS cluster. We note that this process is likely to be responsible for the changes in the $P_{1/2}$ parameter of the FeS cluster reported earlier in the mitochondrial system (*40*).

ESE Decay of the FeS Cluster in Wild-Type Cytochrome bc_1 and the FeS Motion Knockout in the Absence and Presence of Various Inhibitors. The magnetic interaction between the two paramagnetic centers decreases with third power as the distance between the centers increases (*33*). In our case, one of the centers (the FeS cluster) naturally undergoes a large-scale movement, while the other (heme b_L) remains immobile (Figure 1a). Thus, the enhancement of phase relaxation of the FeS cluster induced by the relaxation of heme b_L identified in the experiments shown in Figure 5 is expected to reflect the equilibrium distance distribution of the FeS head domain. The stigmatellin-induced state, as the state with well-defined and unchanging in time approximately 2.6 nm distance between the FeS cluster and the iron of heme b_L (Figure 1a), sets the level of the enhancement to which other states can be compared.

In native, noninhibited cytochrome bc_1, the observed enhancement is significantly weaker. This is expressed in much lower value of the local maximum of the temperature dependence of $1/T_M$ for the ascorbate-reduced sample (Figure 6a) and, consequently, in smaller value of the integrated area under the curve (Figure 8a). This latter parameter, calculated from the fitted functions to ascorbate minus dithionite temperature dependences of $1/T_M$ as described in Experimental Procedures, appears as an additional empirical parameter that conveniently compares the strength of dipolar relaxation; the larger the value of the integrated area under the curve, the stronger the dipolar enhancement of phase relaxation.

The treatment of cytochrome bc_1 with the Q_o- or Q_i-site inhibitor, myxothiazol or antimycin, respectively, leads to further weakening of the enhancement, if compared to the noninhibited enzyme, however, the degree of the weakening depends on the type of inhibitor used. The change induced by the presence of myxothiazol is small yet detectable (Figure 6b). The effect is more pronounced in the case of antimycin, where a flattening of the temperature dependence of $1/T_M$ for the ascorbate-reduced sample (Figure 6c) leads to a clear decrease in the integrated area under the curve (Figure 8a). The sample treated with myxothiazol and antimycin shows the most flattened temperature dependence of $1/T_M$ (Figure 6d) and the smallest value of the integrated area (Figure 8a). Clearly, the effects due to the presence of myxothiazol and antimycin on the enhancement are additive.

We thus observe that the enhancement of the phase relaxation is less effective in the samples that were not treated with stigmatellin. In these samples the FeS head domain position is not fixed, and its large scale movement can significantly modulate the distance between the FeS cluster and heme b_L. This weakens the measured strength of dipolar interaction between the two metal centers.

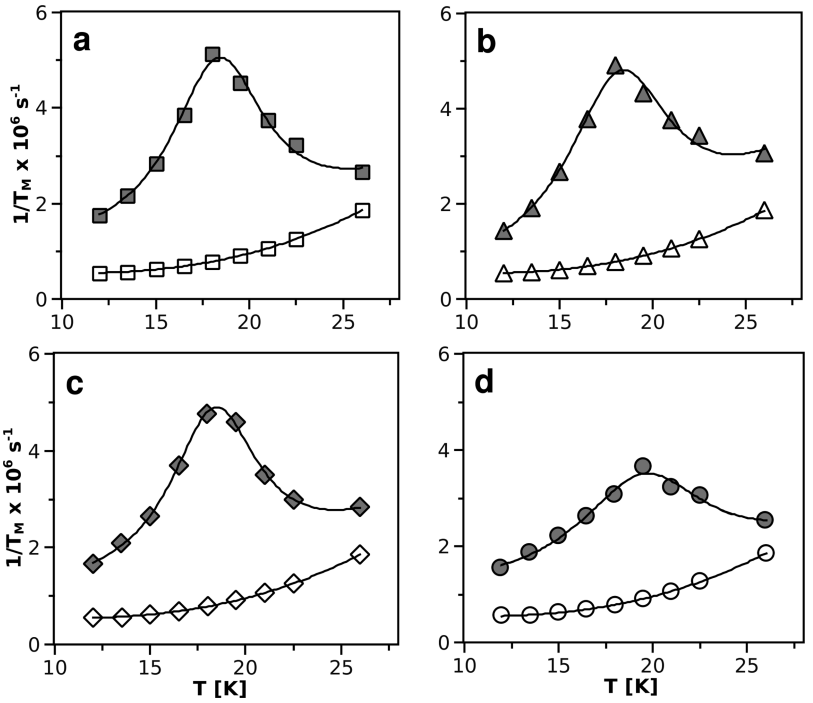

FIGURE 7: Comparison of the effect of inhibitors on the temperature dependence of phase relaxation rate of the FeS cluster in the FeS motion knockout. Shown are data for ascorbate-reduced (closed symbols) and dithionite-reduced (open symbols) samples of noninhibited cytochrome bc_1 (a) and enzyme inhibited with myxothiazol (b), antimycin (c), or stigmatellin (d).

The assumption about the ability of the FeS head domain to move is rationalized kinetically. In the native, noninhibited enzyme it is an inherent part of a whole catalysis. In the myxothiazol or antimycin-inhibited enzyme it is a part of the residual activity; even though the two inhibitors block two different catalytic sites, they do not break the diffusional communication of the FeS cluster with heme c_1.

The correlation between the level of the enhancement and the distance distribution of the FeS head domain is further evident in the experiments performed with the FeS motion knockout. In this form, a + 2Ala mutational insertion in the neck region connecting the FeS head domain with the hydrophobic anchor imposes structural constraints and severely impedes the motion arresting the FeS head domain in the Q_o site for seconds (*20*). Thus, as expected, the enhancement of FeS cluster relaxation in this mutant is generally very strong (Figures 7 and 8b). Without any inhibitor added the level of the enhancement even exceeds that observed in the wild-type enzyme treated with stigmatellin (Figure 7a). Addition of antimycin or myxothiazol does not change the level of the enhancement (Figure 7b or 7c, respectively). On the other hand, addition of stigmatellin lowers the level so that it approaches the level of stigmatellin-treated wild-type cytochrome bc_1 (Figure 7d).

To understand the origin of a decrease in the level of enhancement in the FeS motion knockout treated with stigmatellin, it is necessary to take into account that the local maximum of the temperature dependence of $1/T_M$ is shifted by more than 1 K (from approximately 18.3 to 19.5 K, Table S1 in Supporting Information). The similar shift is observed in wild-type cytochrome bc_1 treated with stigmatellin (Table S1 in Supporting Information). Such shifts of the local maxima may be related with changes in a dipolar splitting associated with alteration of g tensor values (only samples treated with stigmatellin show a clear shift of g_y from 1.90 to 1.89) and of relative orientations of magnetic axes in relation to molecular axes, reminiscent of structural alterations within the cluster that might have been necessary to accommodate the binding of stigmatellin. This modification of intrinsic properties of the cluster (shift in the temperature optimum) may be just enough to cause an apparent weakening of the enhancement expressed as the integrated area under the curve. It thus appears that the upper level of the enhancement for the FeS cluster at the Q_o site is most adequately represented by the level seen in the FeS motion knockout without stigmatellin added. To illustrate this, a correction accounting for the effect of stigmatellin was included in Figure 8 (gray part of the bars for stigmatellin).

Dipolar Relaxation Part of ESE Decay Curves of the FeS Cluster. To get further insights into the possible origin of the variations in the enhancement seen in different samples, we performed a detailed analysis of pure dipolar decay curves (see Experimental Procedures for details). Dipolar traces obtained for native cytochrome bc_1 at 12 K in the absence and presence of inhibitors are shown in Figure 9a. At this temperature all traces are well described by the single exponent function, but the time constant of each decay and the offset are different. The sample treated with stigmatellin (Figure 9a, black trace) exhibits the fastest dipolar decay with the very small offset (the curve goes to zero). The samples that were not treated with stigmatellin show increase in both the time constant (slower decay) and the offset. Those increases follow the order noninhibited, myxothiazol-treated, antimycin-treated, antimycin plus myxothiazol-treated samples (Figure 9a, gray traces).

In contrast to the native cytochrome bc_1, the dipolar relaxation of the FeS cluster in the FeS motion knockout is not sensitive to the presence or absence of inhibitors. As shown in Figure 9b all of the traces are similar, with the time constants and the offsets almost identical to those obtained for native cytochrome bc_1 treated with stigmatellin (see Figure 9a, black trace).

To understand the origin of the offset in the dipolar decay curves, one should bear in mind that the experimentally obtained

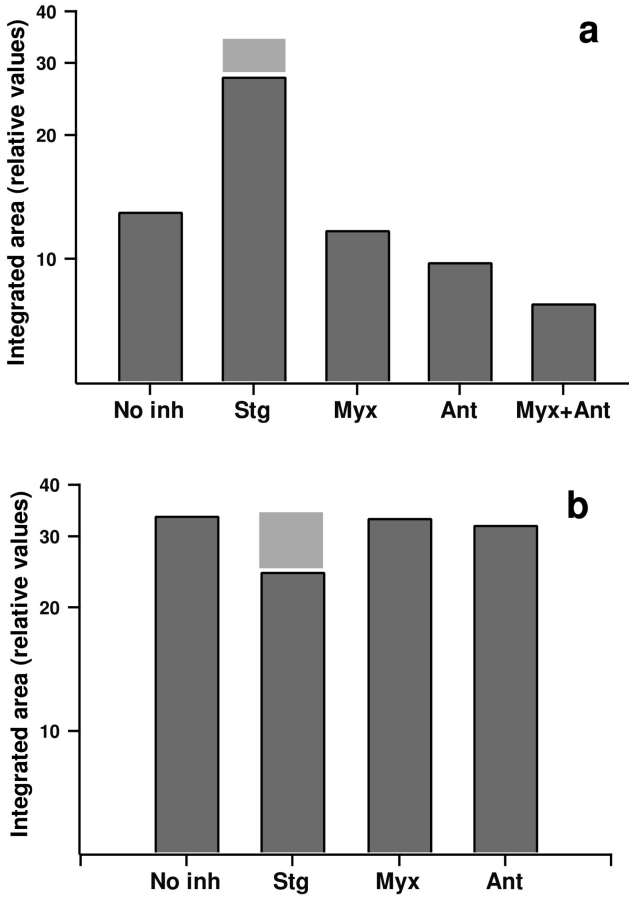

FIGURE 8: Comparison of the level of relaxation enhancement of the FeS cluster in cytochrome bc_1 in the presence and absence of inhibitors. The level of the enhancement in native cytochrome bc_1 (a) and the FeS motion knockout (b) is expressed as the integrated area under the curves obtained from subtraction of temperature dependences of $1/T_M$ for dithionite-reduced samples from those for ascorbate-reduced samples. Abbreviations: No inh, Stg, Myx, Ant, and Myx + Ant denote the samples without inhibitor and with stigmatellin, myxothiazol, antimycin, and myxothiazol plus antimycin, respectively. Gray bar illustrates a correction accounting for the apparent weakening of the enhancement caused by stigmatellin (see Results for details).

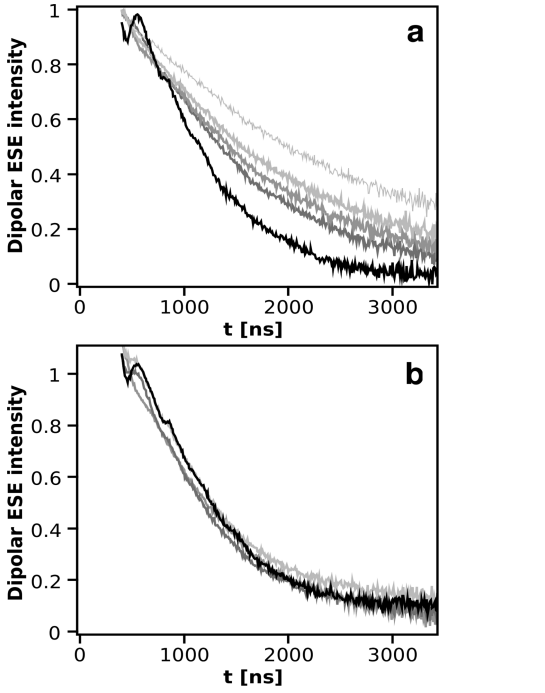

FIGURE 9: Pure dipolar decay curves of the FeS cluster obtained from Q-band measurements at 12 K in the presence and absence of inhibitors. (a) shows dipolar decays in native cytochrome bc_1. The gray scale illustrates a progressive weakening of the phase relaxation which follows the order stigmatellin (black), noninhibited (dark gray), myxothiazol-treated (intermediate gray), antimycin-treated (gray), and myxothiazol plus antimycin-treated (light gray) cytochrome bc_1. (b) shows dipolar decays in the FeS motion knockout. Color code is as in (a).

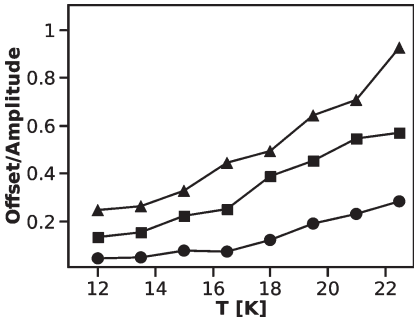

FIGURE 10: Temperature dependence of the offset in the dipolar decay curves of native cytochrome bc_1 determined for noninhibited (squares) and stigmatellin- (circles) or myxothiazol plus antimycin-treated (triangles) samples.

traces represent a part of the whole decay due to the cutoff from both the beginning and the end of the curve. The large portion of the fastest dipolar decays is completed within the spectrometer dead time t_{dead} (400 ns in our case) and thus is represented only as reduced amplitude of the echo. On the other hand, the relatively short intrinsic phase relaxation of the FeS cluster cuts off the slower parts of the decays leading to the "experimental" offset in divided curves (the longest, 3500 ns, curve is recorded at 12 K and the other curves become gradually shorter as the temperature increases).

A physical meaning can be attributed to this offset when the temperature dependence of dipolar decay is analyzed in the context of the distribution of angles and distances $\Delta(r, \theta)$ inherent to powder spectra (Figure S2, Supporting Information). A typical decay curve contains the fast- and slow-relaxing components. For the spins with gradually increasing distance r, the dipolar relaxation becomes slower, and their contribution to the tail of the echo decay curve is more significant. Thus, at the point of the experimental cutoff (which, as mentioned above, is different for each temperature) the level of the offset is proportional to the number of slowly relaxing spins (more distant from heme b_L).

Indeed, the smallest changes in the offset are observed for native enzyme treated with stigmatellin (Figure 10, circles) and the FeS motion knockout (data not shown), which is expected for the sample with a largest population of spins close to heme b_L and impacted by the strongest enhancement of relaxation. For other samples the increase in the offset with temperature is larger (Figure 10, squares and triangles), which can be explained by assuming that a population of spins more distant from heme b_L becomes larger, leading to an increase in the fraction of slower dipolar decays. This reasoning is supported by the simulations of the dipolar traces. Figure 11 compares the dipolar relaxation curves of the cluster calculated for $r = 2.64$ nm (Q_o position) and $r = 3.55$ nm (c_1 position). Clearly, the position more distant from heme b_L (in this case the c_1 position) produces greater offset in the dipolar curve if the cutoff of 3000 ns is applied.

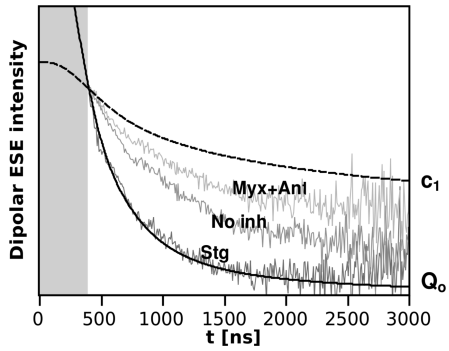

FIGURE 11: Comparison of the simulated and experimental dipolar traces of the FeS cluster in native cytochrome bc_1. Experimental dipolar decay curve for stigmatellin-treated cytochrome bc_1 at 19.5 K (Stg) is best fitted with the spin−lattice relaxation rate of heme b_L of 4×10^6 s^{-1}, when $r = 2.64$ nm and $\sum\Delta_A(\theta)$ is calculated from the crystal structure of cytochrome bc_1 (see Figure S2 in Supporting Information) with the FeS in position A. If the same spin−lattice relaxation rate of heme b_L is taken, a simulation using $r = 3.55$ nm and $\sum\Delta_D(\theta)$ calculated from the crystal structure of position D (see Figure S2 in Supporting Information) yields the dipolar curve for the FeS cluster in the single c_1 position (dotted line). Experimental dipolar decay curves for noninhibited (No inh) and antimycin plus myxothiazol-treated (Myx + Ant) cytochrome bc_1 are also shown. Gray area denotes the spectrometer dead time (0 on the t scale denotes the beginning of the relaxation).

We thus conclude that this additional increase in the offset reflects a shift in a density of the FeS cluster toward positions more distant from heme b_L (the Q_o site). All of those observations are consistent with the results obtained from phenomenological analysis of $1/T_M$ vs temperature (Figures 6−8). The weakening of the enhancement (reminiscent of increase in the distance between the FeS cluster and heme b_L) is present in the same samples that show the additional increase in the offset.

The simulated traces shown in Figure 11 represent the two boundary levels to which the experimental traces can now be compared. The trace recorded for cytochrome bc_1 treated with stigmatellin fits well with a simulation for the Q_o position. This is consistent with the notion that in this sample a single population of FeS with $r = 2.64$ nm is present. On the other hand, the traces recorded for other wild-type cytochrome bc_1 samples place themselves in between the two boundary levels, as exemplified for the noninhibited and myxothiazol plus antimycin-treated samples (Figure 11). None of those traces, even that coming from the sample with the weakest enhancement (myxothiazol plus antimycin-treated sample), appear to fit the level simulated for a single population of FeS with $r = 3.55$ nm (c_1 position).

We thus observe that different samples of native cytochrome bc_1 in the absence of stigmatellin produce distinct dipolar decay curves, but all of the curves fall between the calculated boundary levels defined for the Q_o and c_1 positions. To understand these results, we calculated dipolar decays for defined crystal positions A−D (see Experimental Procedures) at different temperatures (i.e., for different T_1 of heme b_L). As shown in Figure S3 (Supporting Information), the decays for the single positions A, B, and C differ only slightly between themselves, while the decay for the position D clearly stands out from those calculated for the other (A−C) positions, even at low temperatures (for long T_1 of heme b_L). Thus, the observed differences in the experimental dipolar decays of samples of native cytochrome bc_1 in the absence of stigmatellin (Figure 11) must originate mainly from the different contribution of the occupancy of position D in respect to the occupancy of the other positions. This implicates the presence of a broad distribution of FeS positions in those samples.

DISCUSSION

The experimental difficulties with direct observation of the motion of the FeS head domain set the stage at which most information about this phenomenon comes from extrapolations of the results coming from indirect structural studies. These studies, mostly crystallography or CW EPR of oriented membranes, follow a common approach of analyzing a collective effect of identically oriented macromolecules bound to macroscopic property of the ordered sample. We, however, have undertaken a quite different approach which benefited from the intrinsic property of the protein that appeared traceable by pulse EPR. This allowed us to analyze macroscopically disordered individuals that all have the intrinsic feature not connected to any of the macroscopic property of the sample.

This intrinsic property is a magnetic interaction between the reduced FeS cluster and oxidized heme b_L. Our analysis of this interaction based on a comparison of different samples of cytochrome bc_1 (without and with stigmatellin or the mutation fixing the position of FeS head domain at the Q_o site) under the same redox state of cofactors (reduced FeS cluster and oxidized heme b_L) revealed that an extent of a dipolar enhancement of phase relaxation of the cluster is a particularly sensitive parameter reflecting a position of the cluster with respect to heme b_L. The experimentally measured changes in the enhancement are strictly related to changes in distance between those two cofactors with a general simple rule that the closer the FeS cluster to heme b_L is going to be, the stronger the enhancement is going to be observed. This parameter can be regarded as an internal spectroscopic ruler which, unlike in measurements based on CW EPR of the cluster, does not directly depend on the shape and value of the g_x transition. We thus avoid complications arising from the well-known fact that the g_x transition can be modified by a number of factors of different origin (redox state and presence of quinones, inhibitors, solvents, mutations, breakage of disulfide bond, presence of g-strain, and many others) (*25*, *55*, *57*−*59*).

Remarkably, the measured changes in the phase relaxation enhancement provide the first direct experimental description of changes in dipolar coupling between the FeS cluster and heme b_L of cytochrome bc_1. A success in those types of experiments is not always guaranteed, as it requires that relatively slow intrinsic spin−lattice and phase relaxation of one center (in our case, the FeS cluster) allows to detect its spin echo in the temperature range where the relaxation rate of the other center (in our case, heme b_L) is comparable to dipolar splitting of the spectra of the first center (the FeS cluster).

The fact that in the measurements we use a glass state of sample generated by a rapid freezing of a protein solution means that we can trap an equilibrium distribution of states that existed in liquid state just before freezing. This is clearly an advantage over other methods that require drying or crystallization of the samples and provides us with a new perspective on looking into the motional behavior of the FeS head domain.

Origin of Changes in the FeS−Heme b_L Distance Distribution. The comparison of the measured dipolar relaxation curves with the curves calculated for the FeS cluster occupying distinct positions (as defined by crystallography) revealed that noninhibited native cytochrome bc_1 under the applied experimental conditions (isolated enzyme without externally added

quinones) maintains a broad distribution of distances between the FeS cluster and heme b_L (positions of the FeS head domain). It also demonstrated that the average equilibrium position is modifiable by inhibitors or mutations. In our view, a diffusion-based mode of the motion of the FeS head domain is sufficient to adequately describe those observations.

In this model, the changes in the equilibrium distribution of the positions of the FeS head domain are induced by modifications of the orienting potential gradient in which constrained diffusion of the FeS head domain takes place (*60*−*62*). In the stigmatellin-induced state, a creation of the hydrogen bond between the inhibitor and one of the histidines coordinating the FeS cluster eliminates the possibility of the FeS head domain to move (i.e., the potential barrier for diffusing out of the Q_o site is much larger than thermal energy). This is associated with the strongest observable enhancement. In all other states of native enzyme (i.e., in the absence of stigmatellin), the FeS head domain moves in and out of the Q_o site, which shifts its average equilibrium position. The density of the FeS head domain at Q_o site diminishes (in comparison to the stigmatellin-induced state), which generally is accompanied by a decrease in the measured relaxation enhancement.

In the absence of any inhibitor, the average equilibrium position of the FeS head domain is shifted, if compared to the stigmatellin-induced state, toward the c_1 position, as the level of enhancement indicates (it is between the two boundary levels of Figure 11). Addition of myxothiazol induces some (even small) structural changes (*19*, *63*) that slightly modify the orienting potential gradient and shift the average equilibrium position more toward the c_1 position (the observed enhancement is slightly weaker, in comparison to noninhibited enzyme; Figures 6b and 8a). In the presence of antimycin, the modification of the orienting potential gradient appears to be larger, leading to the further shift in the average equilibrium position toward the c_1 position (the observed enhancement is weaker, in comparison to myxothiazol-treated enzyme; Figures 6c and 8a). In the presence of both myxothiazol and antimycin the modification of the orienting potential gradient appears to be largest (the observed enhancement is weakest; Figures 6d and 8a). This additivity suggests that structural effects of myxothiazol and antimycin are of different origin and independently contribute to the modification of the orienting potential gradient.

In the FeS motion knockout, a creation of steric barrier locks the FeS head domain at the Q_o site for seconds (*20*), but the occasional motion toward the cytochrome c_1 still occurs, as reflected by the residual enzymatic activity (*64*). This means that the potential barrier is somewhat lower from that of the stigmatellin-induced state. Nevertheless, it is still significant, in comparison to the thermal energy; thus at a given time almost the entire population of the FeS clusters occupies positions at the Q_o site. Consequently, the observed enhancement is similar to that seen in the stigmatellin-induced state. The mutational effect dominates any of possible changes induced by myxothiazol or antimycin (described earlier for the native enzyme), as reflected by lack of observable change in the enhancement (Figures 7, 8b, and 9b).

It is important to bear in mind that the presented comparison is relevant to only a specific redox state of the enzyme (the FeS cluster reduced and heme b_L oxidized). This limitation is due to the fact that the electron spin of the FeS cluster does not sense diamagnetic heme b_L. Consequently, the profiles of the temperature dependence of the phase relaxation rate of FeS cluster in all samples having the heme reduced (regardless of the absence or presence of inhibitors or mutations) are virtually the same (Figures 6 and 7, open symbols). In another words, the intrinsic phase relaxation of the FeS cluster in any conformation (or an ensemble of conformations) in the absence of dipolar interaction is the same. This does not preclude a, rather unlikely in our view, possibility that conformational changes, such as change in positional distribution of FeS head domain, upon reduction of heme b_L occur. The method simply cannot detect them. Neither the method detects the states with the oxidized FeS cluster that so far have only been accessed by cryoreduction combined with EPR measurements (*24*).

Relating the Effects of Myxothiazol and Antimycin to Other Studies. While the crystallographic data suggest increased mobility of the FeS head domain in the presence of myxothiazol (*3*, *19*, *63*, *65*), the structural effects of the presence of antimycin are much less clear (*66*, *67*). On the other hand, the EPR studies of oriented membranes indicate an increased disorder of the FeS cluster orientations in the presence of either of the inhibitors (*23*, *26*, *27*). Our results are generally consistent with those observations. It now becomes clear that those inhibitors can affect the average equilibrium position of the FeS head domain. The direction of the change (the observed shifts toward the c_1 position) implicates a decrease in density of the FeS cluster at the Q_o site which, as judged from the differences in the extents of the effects, appears to be more pronounced in the case of antimycin than in the case of myxothiazol. Remarkably, the antimycin-induced shift may in part contribute to the elevated levels of superoxide generation routinely observed with the enzyme treated with this inhibitor. This would be in line with our recent proposal that the movement of the FeS center transiently "opens" the Q_o site for reaction with oxygen in what should be regarded as a kinetic effect of slowing certain reactions supported by the FeS center (*64*). According to this mechanism, leaks of single electrons to oxygen are most probable when the two chains of cytochrome bc_1 are saturated with electrons and the FeS center is not at the Q_o site to immediately participate in the Q_o site reactions (*64*). Thus, the conditions of increased probability of leaks are likely to intensify as the density of the FeS center shifts toward the c_1 position while electrons cannot travel freely due to the blockage of the Q_i site.

The shift associated with the presence of antimycin is also interesting from a structural point of view, as it shows the influence of inhibitor that binds to the site remote from the region occupied by the FeS head domain. This finding appears consistent not only with the mentioned earlier antimycin-induced dissipation of the angular dependence of the EPR ordered membrane spectra (*23*, *27*) but also with the observation about the increased proteolysis of the FeS subunit in response to the Q_i site inhibitors (*68*). We note that those types of observations gave rise to the models that evoke an allosteric influence of the state of the Q_i site on the operation of the Q_o site (*27*, *69*, *70*). At present, however, it is not clear to what extent the changes induced by inhibitors reproduce or resemble the states encountered by the enzyme during catalysis. Establishing this as well as understanding the meaning of the changes in the dynamic distribution of the positions of the FeS head domain in the context of the mechanism of the operation of cytochrome bc_1 awaits further studies. We anticipate that they will greatly benefit from the fact that, with the new approach presented here, it is now feasible to directly monitor changes in distance between the FeS cluster and heme b_L in frozen solution under many different experimental conditions.

ACKNOWLEDGMENT

We thank Prof. Fevzi Daldal (University of Pennsylvania, Philadelphia, PA) for providing us with the *R. capsulatus* strains (wild-type and mutant strains) used in this work and Prof. P. Leslie Dutton (University of Pennsylvania, Philadelphia, PA) for valuable discussions.

SUPPORTING INFORMATION AVAILABLE

Definition of A, B, C, and D positions of the FeS cluster; values of relative dipolar splitting calculated for FeS positions A and D; simulated dipolar decays for FeS positions A−D for different relaxation rates of heme b_L; local maxima of phase relaxation enhancement. This material is available free of charge via the Internet at http://pubs.acs.org.

REFERENCES

1. Berry, E. A., Guergova-Kuras, M., Huang, L., and Crofts, A. R. (2000) Structure and function of cytochrome *bc* complexes. *Annu. Rev. Biochem. 69*, 1005–1075.
2. Xia, D., Yu, C. A., Kim, H., Xia, J. Z., Kachurin, A. M., Zhang, L., Yu, L., and Deisenhofer, J. (1997) Crystal structure of the cytochrome bc_1 complex from bovine heart mitochondria. *Science 277*, 60–66.
3. Iwata, S., Lee, J. W., Okada, K., Lee, J. K., Iwata, M., Rasmussen, B., Link, T. A., Ramaswamy, S., and Jap, B. K. (1998) Complete structure of the 11-subunit bovine mitochondrial cytochrome bc_1 complex. *Science 281*, 64–71.
4. Zhang, Z., Huang, L., Shulmeister, V. M., Chi, Y. I., Kim, K. K., Hung, L. W., Crofts, A. R., Berry, E. A., and Kim, S. H. (1998) Electron transfer by domain movement in cytochrome bc_1. *Nature 392*, 677–684.
5. Hunte, C., Koepke, J., Lange, C., Roβmanith, T., and Michel, H. (2000) Structure at 2.3 Å resolution of the cytochrome bc_1 complex from the yeast *Saccharomyces cerevisiae* co-crystalized with an antibody F_v fragment. *Structure 8*, 669–684.
6. Berry, E. A., Huang, L.-S., Saechao, L. K., Pon, N. G., Valkova-Valchanova, M. B., and Daldal, F. (2004) X-ray structure of *Rhodobacter capsulatus* cytochrome bc_1: comparison with its mitochondrial and chloroplast counterparts. *Photosynth. Res. 81*, 251–275.
7. Esser, L., Elberry, M., Zhou, F., Yu, C. A., and Xia, D. (2008) Inhibitor-complexed structures of the cytochrome bc_1 from the photosynthetic bacterium *Rhodobacter sphaeroides*. *J. Biol. Chem. 283*, 2846–2857.
8. Kurisu, G., Zhang, H., Smith, J. L., and Cramer, W. A. (2003) Structure of the cytochrome b_6f complex of oxygenic photosynthesis: tuning the cavity. *Science 302*, 1009–1014.
9. Stroebel, D., Choquet, Y., Popot, J.-L., and Picot, D. (2003) An atypical haem in the cytochrome b_6f complex. *Nature 426*, 413–418.
10. Mitchell, P. (1975) The protonmotive Q cycle: a general formulation. *FEBS Lett. 59*, 137–139.
11. Osyczka, A., Moser, C. C., Daldal, F., and Dutton, P. L. (2004) Reversible redox energy coupling in electron transfer chains. *Nature 427*, 607–612.
12. Rich, P. R. (2004) The quinone chemistry of *bc* complexes. *Biochim. Biophys. Acta 1658*, 165–171.
13. Osyczka, A., Moser, C. C., and Dutton, P. L. (2005) Fixing the Q cycle. *Trends Biochem. Sci. 30*, 176–182.
14. Cape, J. L., Bowman, M. K., and Kramer, D. M. (2006) Understanding the cytochrome *bc* complexes by what they don't do. The Q cycle at 30. *Trends Plant Sci. 11*, 46–55.
15. Crofts, A. R. (2006) Proton pumping in the bc_1 complex: a new gating mechanism that prevents short circuits. *Biochim. Biophys. Acta 1757*, 1019–1034.
16. Mulkidjanian, A. Y. (2005) Ubiquinol oxidation in the cytochrome bc_1 complex: reaction mechanism and prevention of short-circuiting. *Biochim. Biophys. Acta 1709*, 5–34.
17. Darrouzet, E., Moser, C. C., Dutton, P. L., and Daldal, F. (2001) Large scale domain movement in cytochrome bc_1: a new device for electron transfer in proteins. *Trends Biochem. Sci. 26*, 445–451.
18. Brandt, U. (1998) The chemistry and mechanics of ubihydroquinone oxidation at center P (Q_o) of the cytochrome bc_1 complex. *Biochim. Biophys. Acta 1365*, 261–268.
19. Esser, L., Quinn, B., Li, Y. F., Zhang, M., Elberry, M., Yu, L., Yu, C. A., and Xia, D. (2004) Crystallographic studies of quinol oxidation site inhibitors: a modified classification of inhibitors for the cytochrome bc_1 complex. *J. Mol. Biol. 341*, 281–302.
20. Darrouzet, E., Valkova-Valchanova, M. B., Moser, C. C., Dutton, P. L., and Daldal, F. (2000) Uncovering the [2Fe2S] domain movement in cytochrome bc_1 and its implications for energy conversion. *Proc. Natl. Acad. Sci. U.S.A. 97*, 4567–4572.
21. Darrouzet, E., and Daldal, F. (2002) Movement of the iron-sulfur subunit beyond the *ef* loop of cytochrome *b* is required for multiple turnovers of the bc_1 complex but not for single turnover Q_o site catalysis. *J. Biol. Chem. 277*, 3471–3476.
22. Xiao, K., Yu, L., and Yu, C. A. (2000) Confirmation of the involvement of protein domain movement during the catalytic cycle of the cytochrome bc_1 complex by the formation of an intersubunit disulfide bond between cytochrome *b* and the iron-sulfur protein. *J. Biol. Chem. 275*, 38597–38604.
23. Cooley, J. W., Ohnishi, T., and Daldal, F. (2005) Binding dynamics at the quinone reduction (Q_i) site influence the equilibrium interactions of the iron-sulfur protein and hydroquinone oxidation (Q_o) site of the cytochrome bc_1 complex. *Biochemistry 44*, 10520–10532.
24. Brugna, M., Rodgers, S., Schricker, A., Montoya, G., Kazmeier, M., Nitschke, W., and Sinning, I. (2000) A spectroscopic method for observing the domain movement of the Rieskie iron-sulfur protein. *Proc. Natl. Acad. Sci. U.S.A. 97*, 2069–2074.
25. Roberts, A. G., Bowman, M. K., and Kramer, D. M. (2002) Certain metal ions are inhibitors of cytochrome b_6f complex "Rieske" iron-sulfur protein domain movements. *Biochemistry 41*, 4070–4079.
26. Cooley, J. W., Roberts, A. G., Bowman, M. K., Kramer, D. M., and Daldal, F. (2004) The raised midpoint potential of the [2Fe2S] cluster of cytochrome bc_1 is mediated by both the Q_o site occupants and the head domain position of the Fe-S protein subunit. *Biochemistry 43*, 2217–2227.
27. Cooley, J. W., Lee, D.-W., and Daldal, F. (2009) Across membrane communication between the Q_o and Q_i active sites of cytochrome bc_1. *Biochemistry 48*, 1888–1899.
28. Hung, S. C., Grant, C. V., Peloquin, J. M., Waldeck, A. R., Britt, R. D., and Chan, S. I. (2000) Electron spin-lattice relaxation measurement of the 3Fe-4S (S-3) cluster in succinate:ubiquinone reductase from *Paracoccus denitrificans*. A detailed analysis based on a dipole-dipole interaction model. *J. Phys. Chem. A 104*, 4402–4412.
29. Kulikov, A. V., and Likhtenshtein, G. I. (1977) The use of spin relaxation phenomena in the investigation of the structure of model and biological systems by the method of spin labels. *Adv. Mol. Relax. Interact. Processes 10*, 47–69.
30. Goodman, G., and Leigh, J. S. (1985) Distance between the visible copper and cytochrome *a* in bovine heart cytochrome oxidase. *Biochemistry 24*, 2310–2317.
31. Hirsh, D. J., Beck, W. F., Innes, J. B., and Brudvig, G. W. (1992) Using saturation-recovery EPR to measure distances in proteins: applications to photosystem II. *Biochemistry 31*, 532–541.
32. Zhou, Y., Bowler, B. E., Lynch, K., Eaton, S. S., and Eaton, G. R. (2000) Interspin distances in spin-labeled metmyoglobin variants determined by saturation recovery EPR. *Biophys. J. 79*, 1039–1052.
33. Ulyanov, D., Bowler, B. E., Eaton, G., and Eaton, S. S. (2008) Electron-electron distances in spin-labeled low-spin metmyoglobin variants by relaxation enhancement. *Biophys. J. 95*, 5306–5316.
34. Rakowsky, M. H., More, K. M., Kulikov, A. V., Eaton, G. R., and Eaton, S. S. (1995) Time-domain electron paramagnetic resonance as a probe of electron-electron spin-spin interaction in spin-labeled low-spin iron porphyrins. *J. Am. Chem. Soc. 117*, 2049–2057.
35. Fielding, A. J., Usselman, R. J., Watmough, N., Simkovic, M., Frerman, F. E., Eaton, G. R., and Eaton, S. S. (2008) Electron spin relaxation enhancement measurements of interspin distances in human, porcine, and *Rhodobacter* electron transfer flavoprotein-ubiquinone oxidoreductase (ETF-Q_O). *J. Magn. Reson. 190*, 222–232.
36. Fajer, F. G. (2005) Site directed spin labelling and pulsed dipolar electron paramagnetic resonance (double electron-electron resonance) of force activation in muscle. *J. Phys.: Condens. Matter 17*, 1459–1459.
37. Sudha Rao, B. K., Tyryshkin, A. M., Roberts, A. G., Bowman, M. K., and Kramer, D. M. (2000) Inhibitory copper binding site on the spinach cytochrome b_6f complex: implications for Q_o site catalysis. *Biochemistry 39*, 3285–3296.
38. Lyubenova, S., Siddiqui, M. K., Penning, M. J. M., Ludwig, B., and Prisner, T. F. (2007) Protein-protein interactions studied by EPR relaxation measurements: cytochrome *c* and cytochrome *c oxidase*. *J. Phys. Chem. B 11*, 3839–3846.
39. Mamedov, F., Smith, P. J., Styring, S., and Pace, R. J. (2004) Relaxation behavior of the tyrosine Y_D radical in photosystem

II: evidence for strong dipolar interaction with paramagnetic centers in the S_1 and S_2 states. *Phys. Chem. Chem. Phys. 6*, 4890–4896.
40. Ohnishi, T., Schagger, H., Meinhardt, S. W., LoBrutto, R., Link, T. A., and von Jagow, G. (1989) Spatial organization of redox active centers in the bovine heart ubiquinol-cytochrome *c* oxidoreductase. *J. Biol. Chem. 264*, 735–744.
41. Atta-Asafo-Adjei, E., and Daldal, F. (1991) Size of the amino acid side chain at position 158 of cytochrome *b* is critical for an active cytochrome bc_1 complex and for photosynthetic growth of *Rhodobacter capsulatus*. *Proc. Natl. Acad. Sci. U.S.A. 88*, 492–496.
42. Valkova-Valchanova, M. B., Saribas, A. S., Gibney, B. R., Dutton, P. L., and Daldal, F. (1998) Isolation and characterization of a two-subunit cytochrome *b*-c_1 subcomplex from *Rhodobacter capsulatus* and reconstitution of its ubihydroquinone oxidation (Q_o) site with purified Fe-S protein subunit. *Biochemistry 37*, 16242–16251.
43. Williams-Smith, D. L., Bray, R. C., Barber, M. J., Tsopanakis, A. D., and Vincent, S. P. (1977) Changes in apparent pH on freezing aqueous buffer solutions and their relevance to biochemical electron-paramagnetic-resonance spectroscopy. *Biochem. J. 167*, 593–600.
44. Hirsh, D. J., and Brudvig, G. W. (2007) Measuring distances in proteins by saturation-recovery EPR. *Nat. Protoc. 2*, 1770–1781.
45. Telser, J., Hoffman, B. M., LoBrutto, R., Ohnishi, T., Tsai, A. L., Simpkin, D., and Palmer, G. (1987) Evidence for N coordination to Fe in the [2Fe-2S] center in yeast mitochondrial complex III. Comparison with similar findings for analogous bacterial [2Fe-2S] proteins. *FEBS Lett. 214*, 117–121.
46. Huber, M., Lindgren, M., Hammarstrom, P., Martensson, L. G., Carlsson, U., Eaton, G. R., and Eaton, S. S. (2001) Phase memory relaxation times of spin labels in human carbonic anhydrase II: pulsed EPR to determine spin label location. *Biophys. Chem. 94*, 245–256.
47. Eichel, R. A., Granwehr, J., and Schweiger, A. (2003) Measurement of spin-lattice relaxation times in EPR with enhanced orientation selectivity. *J. Magn. Reson. 162*, 380–384.
48. Lindsey, C. P., and Patterson, G. D. (1980) Detailed comparision of the Williams-Watts and Cole-Davidson functions. *J. Chem. Phys. 73*, 3348–3357.
49. Zhidomirov, G. M., and Salikhov, K. M. (1969) Contribution to the theory of spectral diffusion in magnetically diluted solids. *Sov. Phys. JETP 29*, 1037–1040.
50. Salerno, J. C. (1984) Cytochrome electron spin resonance line shapes, ligand fields, and components stoichiometry in ubiquinol-cytochrome *c* oxidoreductase. *J. Biol. Chem. 259*, 2331–2336.
51. Bowman, M. K., Berry, E. A., Roberts, A. G., and Kramer, D. M. (2004) Orientation of the *g*-tensor axes of the Rieske subunit in the cytochrome bc_1 complex. *Biochemistry 43*, 430–436.
52. Stoll, S., and Schweiger, A. (2006) EasySpin, a comprehensive software package for spectral simulation and analysis in EPR. *J. Magn. Reson. 178*, 42–55.
53. Beinert, H. (2000) Iron-sulfur proteins: ancient structures, still full of surprises. *J. Biol. Inorg. Chem. 5*, 2–15.
54. Ding, H., Moser, C. C., Robertson, D. E., Tokito, M. K., Daldal, F., and Dutton, P. L. (1995) Ubiquinone pair in the Q_o site central to the primary energy conversion reactions of cytochrome bc_1 complex. *Biochemistry 34*, 15979–15996.
55. Ding, H., Robertson, D. E., Daldal, F., and Dutton, P. L. (1992) Cytochrome bc_1 complex [2Fe-2S] cluster and its interaction with ubiquinone and ubihydroquinone at the Q_o site: a double-occupancy Q_o site model. *Biochemistry 31*, 3144–3158.
56. Robertson, D. E., Ding, H., Chelminski, P. R., Slaughter, C., Hsu, J., Moomaw, C., Tokito, M., Daldal, F., and Dutton, P. L. (1993) Hydroubiquinone-cytochrome c_2 oxidoreductase from *Rhodobacter capsulatus*: definition of a minimal, functional isolated preparation. *Biochemistry 32*, 1310–1317.
57. Sharp, R. E., Palmitessa, A., Gibney, B. R., Moser, C. C., Daldal, F., and Dutton, P. L. (1998) Non-inhibiting perturbation of the primary energy conversion site (Qo site) in *Rhodobacter capsulatus* ubihydroquinone:cytochrome *c* oxidoreductase (cytochrome bc_1 complex). *FEBS Lett. 431*, 423–426.
58. Froncisz, W., and Hyde, J. W. (1980) Broadening by strains of lines in the *g*-parallel region of Cu^{2+} EPR spectra. *J. Chem. Phys. 73*, 3123–3131.
59. Zu, Y., Fee, J. A., and Hirst, J. (2002) Breaking and re-forming the disulfide bond at the high-potential respiratory-type Rieske [2Fe2S] center of *Thermus thermophilus*: characterization of the sulfhydryl state by protein-film voltammetry. *Biochemistry 41*, 14054–14065.
60. Martínez, M. C., and Torre, J. G. (1987) Brownian dynamics simulation of restricted rotational diffusion. *Biophys. J. 52*, 303–310.
61. Prosser, R. S., and Davis, J. H. (1994) Dynamics of an integral membrane peptide: a deuterium NMR relaxation study of gramicidin. *Biophys. J. 66*, 1429–1440.
62. Budil, D. E., Sale, K. L., Khairy, K. A., and Fajer, P. G. (2006) Calculating slow-motional electron paramagnetic resonance spectra from molecular dynamics using a diffusion operator approach. *J. Phys. Chem. A 110*, 3703–3713.
63. Esser, L., Gong, X., Yang, S., Yu, L., Yu, C. A., and Xia, D. (2006) Surface-modulated motion switch: capture and release of iron-sulfur protein in the cytochrome bc_1 complex. *Proc. Natl. Acad. Sci. U.S.A. 103*, 13045–13050.
64. Borek, A., Sarewicz, M., and Osyczka, A. (2008) Movement of the iron-sulfur head domain of cytochrome bc_1 transiently opens the catalytic Q_o site for reaction with oxygen. *Biochemistry 47*, 12365–12370.
65. Kim, H., Xia, D., Yu, C. A., Xia, J. Z., Kachurin, A. M., Zhang, L., Yu, L., and Deisenhofer, J. (1998) Inhibitor binding changes domain mobility in the iron-sulfur protein of the mitochondrial bc_1 complex from bovine heart. *Proc. Natl. Acad. Sci. U.S.A. 95*, 8026–8033.
66. Gao, X., Wen, X., Esser, L., Quinn, B., Yu, L., Yu, C. A., and Xia, D. (2003) Structural basis for the quinone reduction in the bc_1 complex: a comparative analysis of crystal structures of mitochondrial cytochrome bc_1 with bound substrate and inhibitors at the Q_i site. *Biochemistry 42*, 9067–9080.
67. Huang, L., Cobessi, D., Tung, E. Y., and Berry, E. A. (2005) Binding of the respiratory chain inhibitor antimycin to the mitochondrial bc_1 complex: a new crystal structure reveals an altered intramolecular hydrogen-bonding pattern. *J. Mol. Biol. 351*, 573–597.
68. Valkova-Valchanova, M., Darrouzet, E., Moomaw, C. R., Slaughter, C. A., and Daldal, F. (2000) Proteolytic cleavage of the Fe-S subunit hinge region of *Rhodobacter capsulatus* bc_1 complex: effects of inhibitors and mutations. *Biochemistry 39*, 15484–15492.
69. Covian, R., and Trumpower, B. L. (2008) Regulatory interactions in the dimeric cytochrome bc_1 complex: the advantages of being a twin. *Biochim. Biophys. Acta 1777*, 1079–1091.
70. Mulkidjanian, A. Y. (2007) Proton translocation by the cytochrome bc_1 complexes of phototrophic bacteria: introducing the activated Q-cycle. *Photochem. Photobiol. Sci. 6*, 19–34.